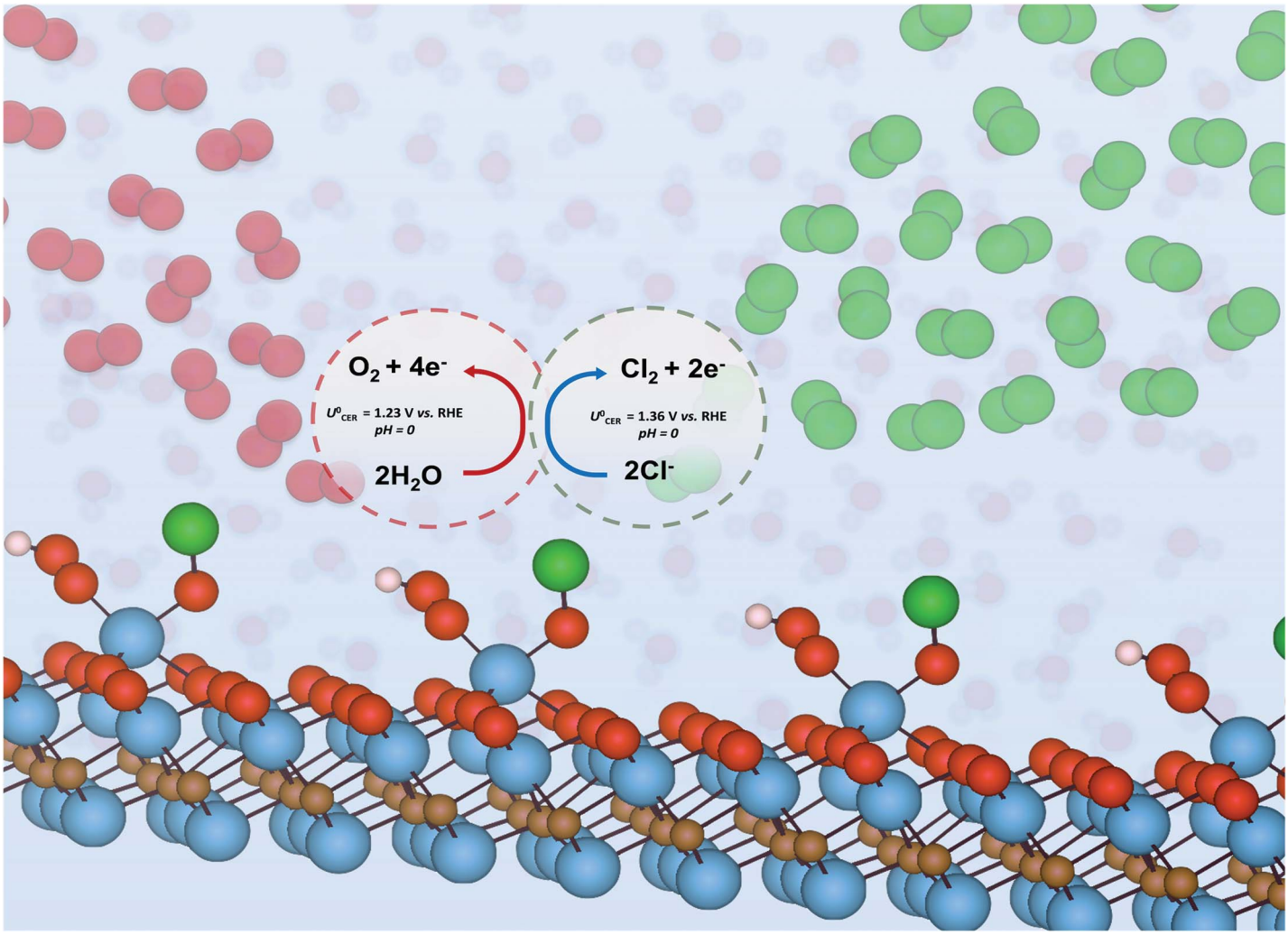

Showcasing research from Professor Exner's laboratory, Faculty of Chemistry, Theoretical Catalysis and Electrochemistry, University of Duisburg-Essen, Essen, Germany.

Trends in competing oxygen and chlorine evolution reactions over electrochemically formed single-atom centers of MXenes

Electrochemically induced surface reconstruction of MXenes forms stable, noble metal-free single-atom centers (SACs) that exhibit structural and functional similarities to archetypal single-atom catalysts. Density functional theory calculations reveal that the *in situ* generated active sites enable selective chlorine evolution under anodic conditions, thus providing a sustainable alternative to noble metal-based catalysts by leading to environmentally friendly and cost-effective chlorine production.

Image reproduced by permission of Shohreh Faridi from *J. Mater. Chem. A*, 2025, **13**, 16481.

As featured in:

See Kai S. Exner *et al.*, *J. Mater. Chem. A*, 2025, **13**, 16481.

ROYAL SOCIETY OF CHEMISTRY

rsc.li/materials-a

Registered charity number: 207890

Journal of Materials Chemistry A

ROYAL SOCIETY OF CHEMISTRY

PAPER

View Article Online
View Journal | View Issue

Cite this: J. Mater. Chem. A, 2025, 13, 16481

Trends in competing oxygen and chlorine evolution reactions over electrochemically formed single-atom centers of MXenes†

Shohreh Faridi, [a] Samad Razzaq, [a] Diwakar Singh, [a] Ling Meng, [b] Francesc Viñes, [b] Francesc Illas [b] and Kai S. Exner [*acd]

Single-atom catalysts (SACs) have garnered widespread attention in the catalysis community due to their ability to catalyze transformations relevant to energy conversion and storage with high activity and selectivity and maximum atomic efficiency. Although considerable efforts are being made to develop synthetic routes for SACs based on non-noble metal atoms, the state-of-the-art SACs are largely based on rare Pt-group metals. MXenes, a new class of two-dimensional materials, offer the exciting possibility of synthesizing single-atom centers with structural similarity to archetypical SACs and without the need for scarce metal atoms such as Pt or Ir. Instead of a dedicated synthetic protocol, only a sufficiently large anodic electrode potential is required to enable the activation of the MXene basal plane by surface oxidation, and the as-formed single-atom centers are sufficiently stable under anodic bias. The electrochemically formed single-atom centers of MXenes based on surface reconstruction differ significantly from previous studies based on SAC sites obtained by doping with foreign metal atoms. In the present work, we demonstrate that the *in situ* formed single-atom centers of MXenes can be effectively used to catalyze energy conversion processes relevant to the chemical industry. By combining electronic structure theory calculations and descriptor-based analysis, we determine activity and selectivity trends in competing oxygen and chlorine evolution reactions and derive activity and selectivity trends for a noble metal-free electrochemical synthesis of gaseous chlorine. Our results indicate that electrochemically formed single-atom centers of two-dimensional materials can play a crucial role for the development of next-generation catalysts for sustainable energy.

Received 19th March 2025
Accepted 4th April 2025

DOI: 10.1039/d5ta02220g

rsc.li/materials-a

Introduction

MXenes are two-dimensional transition-metal carbides and nitrides with the general formula $M_{n+1}X_nT_x$, where M represents a transition metal (Sc, Y, Ti, Zr, Hf, V, Nb, Ta, Cr, Mo, W, or Mn), X is either carbon or nitrogen, and T denotes surface adsorbates (*O, *OH, and *F, among others).[1,2] Since their discovery by Gogotsi and co-workers in 2011,[3] this class of materials has attracted interest in energy conversion and storage due to their excellent electronic conductivity, large surface area, and hydrophilic surfaces combined with their low cost due to the use of non-scarce metals.[4] The application of MXenes even goes beyond the energy sector and includes medical platforms and devices.[5]

In the field of electrocatalysis, two-dimensional materials[6,7] including MXenes are discussed as a potential replacement for traditional Pt-group catalysts.[8–15] The suitability of this class of materials for catalyzing electrochemical transformations was demonstrated back in 2016 by Vojvodic and co-workers,[16] who reported that the basal planes of the MXene Mo_2CT_x are catalytically active toward the hydrogen evolution reaction. In the following years, numerous DFT-based studies investigated the elementary steps of (electro-)catalytic processes on the basal planes of MXenes, with a focus on reactions occurring under cathodic conditions.[17–21] While the MXene basal plane could represent a suitable active site motif for cathodic polarization, the MXene surface reconstructs in contact with water under anodic polarization:[22,23] a surface metal atom is pulled out of the basal plane, and the resulting site is somewhat reminiscent of a single-atom catalyst (*cf.* Fig. 1a). Only recently, it has been demonstrated that this motif formation through surface oxidation is potential dependent,[24] and the as-formed single-atom centers (SACs)[25] are active for the oxygen evolution reaction (OER) — $2\,H_2O \rightarrow O_2 + 4\,H^+ + 4\,e^-$, $U_{OER}{}^0 = 1.23$ V *vs.* RHE

[a]University of Duisburg-Essen, Faculty of Chemistry, Theoretical Catalysis and Electrochemistry, Universitätsstraße 5, 45141 Essen, Germany. E-mail: kai.exner@uni-due.de

[b]Departament de Ciència de Materials i Química Física & Institut de Química Teòrica i Computacional (IQTCUB), Universitat de Barcelona, c/ Martí i Franquès 1-11, 08028 Barcelona, Spain

[c]Cluster of Excellence RESOLV, 44801 Bochum, Germany

[d]Center for Nanointegration (CENIDE) Duisburg-Essen, 47057 Duisburg, Germany

† Electronic supplementary information (ESI) available. See DOI: https://doi.org/10.1039/d5ta02220g

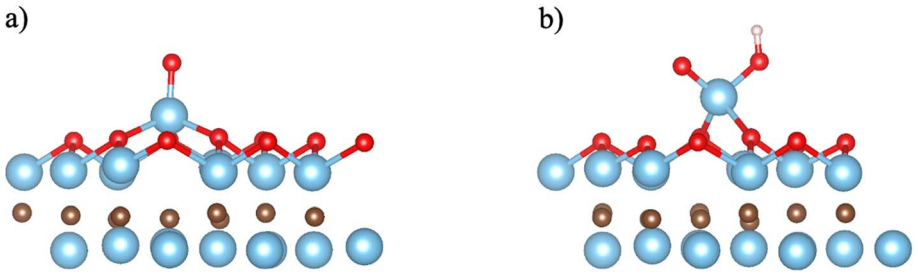

Fig. 1 (a) Single-branch MXene-SAC motif with a single intermediate adsorbed at the out-of-plane metal atom, represented by M_{SAC}-*O. (b) Double-branch MXene-SAC motif with two intermediates adsorbed at the out-of-plane metal atom, represented by M_{SAC}-*O-*OH. Blue, brown, red, and white spheres denote metal, carbon or nitrogen, oxygen, and hydrogen atoms, respectively.

(reversible hydrogen electrode). A clear challenge in (electro-) catalysis is therefore to activate the MXene surface by surface oxidation to enable the formation of the SAC-like sites, although this activation process should not lead to degradation of the material, which would be the case at large anodic potentials. A recent theoretical work for Ti_2CT_x based on *ab initio* molecular dynamics demonstrated that the SAC-like motif is stable at applied electrode potentials up to $U = 1.76$ V *vs.* RHE,[26] which provides a sufficient potential range beyond the equilibrium potential of the OER to catalyze electrochemical transformations under anodic bias. This suggests that the electrochemically formed SAC-like motif of MXenes in the homologous series of M_2X-SAC is a promising candidate for anodic conversion reactions due to its stability under anodic polarization.

In addition to the OER, there is interest in the formation of gaseous chlorine, which is realized industrially by chlor-alkali electrolysis:[27–29] there, the chlorine evolution reaction (CER) — $2\,Cl^- \rightarrow Cl_2 + 2e^-$, $U^0_{OER} = 1.36$ V *vs.* SHE (standard hydrogen electrode) — takes place at the anode, the selectivity of which is impaired by the competing OER. While the introduction of single-atom[30–32] or atomically-dispersed catalysts as anode materials has opened new avenues to direct the selectivity in the competing CER and OER toward the desired product Cl_2,[33] the state-of-the-art catalysts for the CER still rely on Pt-group metals.[34–36] Mixed-metal oxides based on RuO_2, IrO_2, and TiO_2 are combined in dimensionally stable anodes for industrial electrolysis, and the most prominent SAC for the CER refers to a single platinum site doped on a carbon nanotube developed by Joo and co-workers.[37]

In the present manuscript, we suggest the application of electrochemically formed SAC-like sites on the MXene basal plane as a new sustainable pathway for selective chlorine formation to overcome the dependence on scarce platinum group metals. To this end, we report activity and selectivity trends of competing CER and OER over SAC-like sites of twelve different MXenes. All computational details for the application of density functional theory (DFT) are summarized in the following section, while section 2 of the ESI† compiles the relevant SAC-like structures for the investigated M_2XT_x MXenes with ABC stacking[38] under applied bias.

Computational details

In this work, we apply electronic structure calculations in the density functional theory (DFT) framework as implemented in the Vienna *Ab initio* Simulation Package (VASP),[39–41] using the Perdew–Burke–Ernzerhof (PBE) exchange correlation functional[42] combined with Grimme's D3 scheme to account for dispersion effects.[43] Core electron effects on the valence electron density are taken into account by the projector augmented wave (PAW) approach.[44] Valence electron density is expanded in a plane wave basis set with a kinetic energy cutoff of 440 eV. Structural relaxation is systematically achieved through energy minimization, and the total energy convergence and maximum force threshold is set to 10^{-6} eV and 0.01 eV Å^{-1}, respectively. For the integration of the reciprocal space, we employ a $5 \times 5 \times 1$ Γ-centered grid within the Brillouin zone.

To ensure physical isolation of the MXene layers along the direction perpendicular to the surface, a vacuum region with a thickness of at least 12 Å is included in all our models. We have performed test calculations for all the adsorbate species observed under chlorine evolution (CER) and oxygen evolution (OER) reaction conditions (all intermediate structures are listed in eqn (1)–(10) or Fig. 3 of the main text), and it turns out that spin polarization changes adsorption energies by less than 0.02 eV. This is the line with previous works,[45] reporting that spin polarization is not relevant to functionalized MXenes surfaces. For a thorough computational benchmark of the single-atom centers (SAC) formed on MXenes, we refer to our recent work in which we tested different levels of theory.[46] There, we also investigated the electronic structure of the SAC-like motif and found that the formation of the SAC motif does not cause any change in the metallic character of functionalized MXenes.[46]

Besides electronic energies, E_{DFT}, we determine the vibrational frequencies of adsorbate species on the MXene surface in the harmonic approximations, by means of DFT calculations, building and diagonalizing the corresponding block of the Hessian matrix, with elements computed as finite difference of analytical gradients. This allows for the calculation of the zero-point energy and entropy of the reaction intermediates. While the entropic contribution consists of the sum of translational, rotational, and vibrational contributions, for adsorbate species we only use the vibrational frequencies to determine an entropic correction. The equations to calculate zero-point energy (ZPE) and vibrational entropy (S) based on the vibrational frequencies are as follows:

$$E_{ZPE} = \frac{1}{2}\sum_i h\nu_i \quad (1)$$

$$\mathrm{TS} = k_\mathrm{B}T\sum_i^n \left[\frac{\frac{h\nu_i}{k_\mathrm{B}T}}{e^{\frac{h\nu_i}{k_\mathrm{B}T}}-1} - \ln\left(1-e^{\frac{-h\nu_i}{k_\mathrm{B}T}}\right)\right] \quad (2)$$

In the above equation, k_B, h, ν_i, n, and T denote the Boltzmann constant, Planck's constant, frequency of vibration, total number of frequencies, and temperature in Kelvin. Zero-point energy and entropic corrections are needed to derive free energies according to the following relation:

$$G = E_\mathrm{DFT} + E_\mathrm{ZPE} - \mathrm{TS} \quad (3)$$

In the remainder of this article, we discuss free-energy changes, ΔG, for the formation of adsorbate species on the MXene-SAC motif. Note that the free-energy changes obtained from the free energies of eqn (3) refer to $U = 0$ V *vs.* SHE (standard hydrogen electrode) and pH = 0, which is denoted as $\Delta G(0)$. We will make use of this nomenclature in section 4 of the ESI† when we introduce the computational hydrogen electrode (CHE) approach[47] to determine potential-dependent free-energy changes to describe the elementary steps of the CER and OER.

A possible source of error in the chosen PBE + D3 level of theory is the existence of localized d-electrons, which GGA functionals tend to excessively delocalize. This can be avoided by making use of hybrid functionals including a fraction of nonlocal Fock exchange such as PBE0 or HSE06, or through the addition of the somehow empirical onsite two-electron repulsion term U leading to the basis of the PBE + U approach. However, one must advert that the choice of the contribution of Fock exchange in hybrid functionals, and also the range separation parameter in HSE06, or the value for the U parameter in PBE + U remain open issues as discussed elsewhere.[48] Considering that the main goal of this study is to discuss activity and selectivity trends for single-atom centers of MXenes based on the calculation of adsorption free energies, one can safely compare the results obtained using the PBE + D3 level of theory as the main interest refers to free-energy differences rather than absolute values. A discussion of the electronic structure of the SAC-like site of MXenes is provided in section 1 of the ESI.†

Results and discussion

In a previous work, we found that the electrochemically formed SAC-like site of MXenes — the one-branch MXene-SAC motif (*cf.* Fig. 1a) — is able to catalyze the OER and CER with reasonable electrocatalytic activity, whereas the MXene basal plane is inactive for both processes.[46] Previous work by Pacchioni and co-workers[49,50] provides evidence that the surface chemistry of single-atom catalysts often differs from that of traditional bulk materials, as the coordination of intermediates adsorbed to the single-atom site is reminiscent to the coordination of ligands in organometallic chemistry. This can give rise to unconventional intermediates and unconventional reaction mechanisms,[51] and — despite the fact that the electrochemically formed SAC-like sites of MXenes are not typical single-atom catalysts even if they show structural similarity — we witness a similar observation for the MXene-SAC motif. With sufficient anodic bias, it is possible that a second adsorbate is stabilized at the single-atom center, which we refer to as the two-branch MXene-SAC motif (*cf.* Fig. 1b). This finding is also confirmed by the application of *ab initio* molecular dynamics simulations with explicit water molecules[46] (*cf.* Fig. S5 in section 2 of the ESI†).

Using thermodynamic considerations in a Pourbaix-like approach,[45,52–54] we determine the stability region of the two-branch MXene-SAC motif depending on the metal atom of M_2X. While a detailed analysis can be found in section 3 of the ESI,† Fig. 2 illustrates the electrode potential at which the one- and two-branch MXene-SAC motifs are in electrochemical equilibrium. We infer that the two-branch MXene-SAC motif is energetically favored over the one-branch MXene-SAC motif at electrode potentials relevant for the CER and OER; that is, $U \geq 1.40$ V *vs.* RHE. Therefore, we investigate the elementary steps of both anodic processes at the two-branch SAC motif and choose a target potential of $U = 1.40$ V *vs.* RHE for analysis purposes. In this context, we assume that one of these branches catalyzes the OER, whereas the other branch is responsible for the CER (*cf.* Fig. 3).

OER is a four proton-coupled electron transfer process, in which different adsorbates, including the *OH, *O, and *OOH intermediates are formed. Similar to single-atom catalysts, the MXene-SAC motif facilitates the stabilization of unconventional OER intermediates,[55] including η_1–*OO(H) or η_2–*OO(H), which can become part of the catalytic cycle.[46] While the η_2–*OO(H) intermediate is energetically favored in the case of the one-branch MXene-SAC motif,[46] we observe that only the η_1–*OO(H) adsorbate is formed in the case of the two-branch MXene-SAC motif, which we attribute to steric hindrance between the intermediates at the SAC-like site. Therefore, we assess the elementary steps of the OER by the traditional mononuclear mechanism (*cf.* eqn (1)–(4)) or by a Walden-type description[56–58] including the η_1–*OO(H) intermediate (*cf.* eqn (5)–(8)):

$$M_\mathrm{SAC}\text{–*O} + H_2O \rightarrow M_\mathrm{SAC}\text{–*O–*OH} + (H^+ + e^-),\ \Delta G_{1a} \quad (4)$$

$$M_\mathrm{SAC}\text{–*O–*OH} \rightarrow M_\mathrm{SAC}\text{–*O–*O} + (H^+ + e^-),\ \Delta G_{2a} \quad (5)$$

$$M_\mathrm{SAC}\text{–*O–*O} + H_2O \rightarrow M_\mathrm{SAC}\text{–*O–*OOH} + (H^+ + e^-),\ \Delta G_{3a} \quad (6)$$

$$M_\mathrm{SAC}\text{–*O–*OOH} \rightarrow M_\mathrm{SAC}\text{–*O} + (H^+ + e^-) + O_2,\ \Delta G_{4a} \quad (7)$$

$$M_\mathrm{SAC}\text{–*O–*OH} \rightarrow M_\mathrm{SAC}\text{–*O–*O} + (H^+ + e^-),\ \Delta G_{1b} \quad (8)$$

$$M_\mathrm{SAC}\text{–*O–*O} + H_2O \rightarrow M_\mathrm{SAC}\text{–*O–*OOH} + (H^+ + e^-),\ \Delta G_{2b} \quad (9)$$

$$M_\mathrm{SAC}\text{–*O–*OOH} \rightarrow M_\mathrm{SAC}\text{–*O–*OO} + (H^+ + e^-),\ \Delta G_{3b} \quad (10)$$

$$M_\mathrm{SAC}\text{–*O–*OO} + H_2O \rightarrow M_\mathrm{SAC}\text{–*O–*OH} + (H^+ + e^-) + O_2,\ \Delta G_{4b} \quad (11)$$

We note that during the formation of the different intermediate species in the OER, the CER can take place on the second branch of the SAC motif. Therefore, in each elementary step of the OER in Fig. 3, the CER cycle is indicated at the other

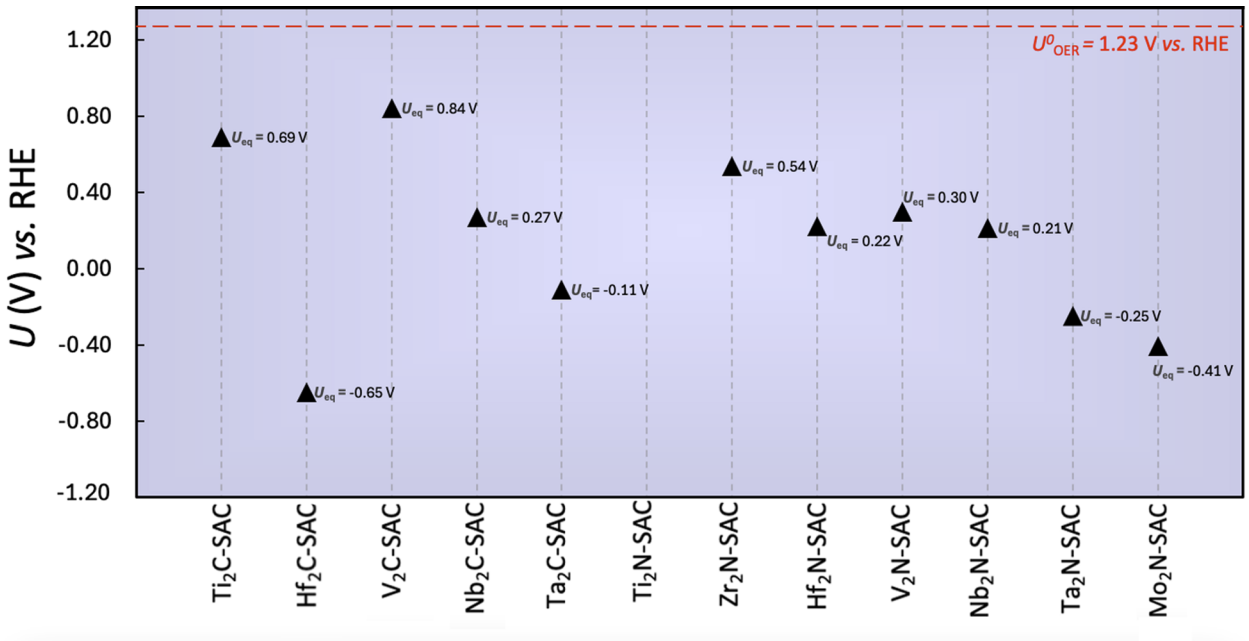

Fig. 2 Equilibrium potential, U_{eq}, of the single-branch (*cf.* Fig. 1a) and double-branch (*cf.* Fig. 1b) MXene-SAC motifs. At potentials exceeding the specified U_{eq} value, the double-branch MXene-SAC motif is energetically favored over the single-branched one, indicating the prevalence of the double-branch MXene-SAC motif under oxygen evolution and chlorine evolution reaction conditions. Please note that Ti_2N is the only MXene among the investigated materials with U_{eq} > 1.23 V and therefore the data point for Ti_2N is not shown in this plot.

branch. In this context, we describe the CER by means of a Volmer–Heyrovsky mechanism:[59]

$$M_{SAC}–*O–*X + Cl^- \rightarrow M_{SAC}–*OCl–*X + e^-, \Delta G_{Vol} \quad (12)$$

$$M_{SAC}–*OCl–*X + Cl^- \rightarrow M_{SAC}–*O–*X + e^- + Cl_2, \Delta G_{Hey} \quad (13)$$

In eqn (9) and (10), *X denotes an arbitrary OER intermediate. The free-energy changes of eqn (1)–(10) are calculated using the computational hydrogen electrode approach, and we

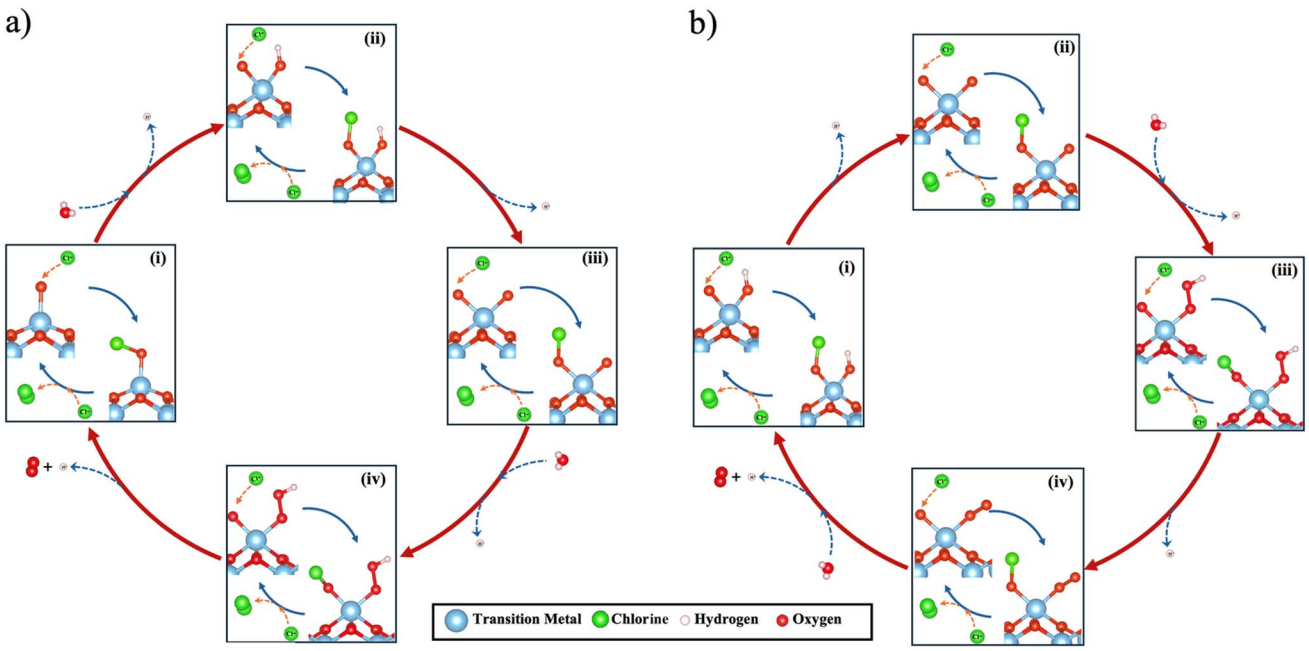

Fig. 3 Schematic representation of the oxygen evolution reaction (OER) over the double-branch MXene-SAC motif *via* two different pathways: (a) mononuclear mechanism, (b) Walden-type mechanism. The competing chlorine evolution reaction is investigated in each step of the OER at the second branch of the SAC site.

refer to section 4 of the ESI† for details (*cf.* Tables S1 and S2†). Knowledge of the OER and CER free-energy changes enables determination of the activity descriptor $G_{max}(U)$ (*cf.* Table S3† in section 4 of the ESI†),[60,61] which is a potential-dependent measure for the electrocatalytic activity based on the energetic span model.[62] A definition of this descriptor for the competing reaction channels of the OER — $G_{max}^{OER}(U)$ — and CER — $G_{max}^{CER}(U)$ — is provided in section 4 of the ESI,† and the energetics of the different mechanisms of eqn (1)–(10) is discussed at $U = 1.40$ V *vs.* RHE in section 5 of the ESI† (*cf.* Fig. S6–S17†).

Since the OER can proceed *via* different reaction mechanisms, we first determine the energetically preferred mechanistic description. This is achieved by comparing the $G_{max}^{OER}(U = 1.40\ V)$ values for the mononuclear (*cf.* eqn (1)–(4)) and Walden-type (*cf.* eqn (5)–(8)) mechanisms for the twelve different M_2X-SAC structures, as shown in Fig. 4. While for the one-branch MXene-SAC motif (*cf.* Fig. 1a) a Walden-type description is energetically favored over the conventional mononuclear mechanism,[46] a different situation is encountered with the two-branch MXene-SAC motif (*cf.* Fig. 1b): a few MXenes follows the traditional mononuclear mechanism, while for some materials (Ta_2C, V_2C, V_2N) both pathways can proceed, and for other materials (Ti_2C, Ti_2N, Zr_2N) the Walden pathway is preferred due to a lower $G_{max}^{OER}(U = 1.40\ V)$ value. This finding suggests that the presence of the second branch modulates the surface chemistry of the SAC site, and this might also have implications for CER activity, evaluated by determining $G_{max}^{CER}(U)$ based on to eqn (9) and (10), and CER selectivity, which is discussed next.

Knowledge of the activity descriptors $G_{max}^{OER}(U = 1.40\ V)$ and $G_{max}^{CER}(U = 1.40\ V)$ for the M_2X-SAC structures allows the determination of the CER selectivity following previous works on this topic:[63]

$$G_{sel}(U) = G_{max}^{OER}(U) - G_{max}^{CER}(U) \quad (14)$$

$$\text{CER selectivity}(U) = \frac{1}{1 + \exp\left(\frac{-G_{sel(U)}}{k_B T}\right)} \quad (15)$$

The results are summarized in Fig. 5, where we provide an activity-selectivity map for the competing CER and OER over two-branch MXene-SAC at $U = 1.40$ V *vs.* RHE. Considering that we calculated the energetics for twelve different MXene-SAC motifs and that there are four different possibilities for the CER for each structure (*cf.* Fig. 3), we arrive at a total of 48 different surface states, which are grouped according to their activity and selectivity in the CER. Relating to selectivity, we distinguish between highly selective (CER selectivity = 1) and non-selective (CER selectivity = 0) motifs, while for CER activity we use $G_{max}^{CER}(U = 1.40\ V) < 0.50$ eV or $G_{max}^{CER}(U = 1.40\ V) \geq 0.50$ eV as a threshold criterion to identify active and inactive surface states, respectively. Note that the selection of these criteria follows previous works on the same topic.[46]

Fig. 5 shows that about 48% (23 out of 48) of all surface states considered are located in the most relevant region with high CER selectivity and high activity (region 1). It becomes clear that in particular the presence of the non-conventional *OO adsorbate on the OER branch enables selective CER, which underlines the similarity of the MXene-SAC motif to archetypal single-atom catalysts in terms of their chemical reactivity. Almost 30% (14 out of 48) of all surface states considered are found in region 2, indicating highly selective CER but reduced CER activity. In particular, the *OH and *OOH adsorbates on the OER branch facilitate selective CER (motif in region 1 or region 2), although the presence of *OH and *OOH is often detrimental to high CER activity (motif in region 2). This is in contrast to the *O and *OO adsorbates, which lead to high CER activity (motif in region 1).

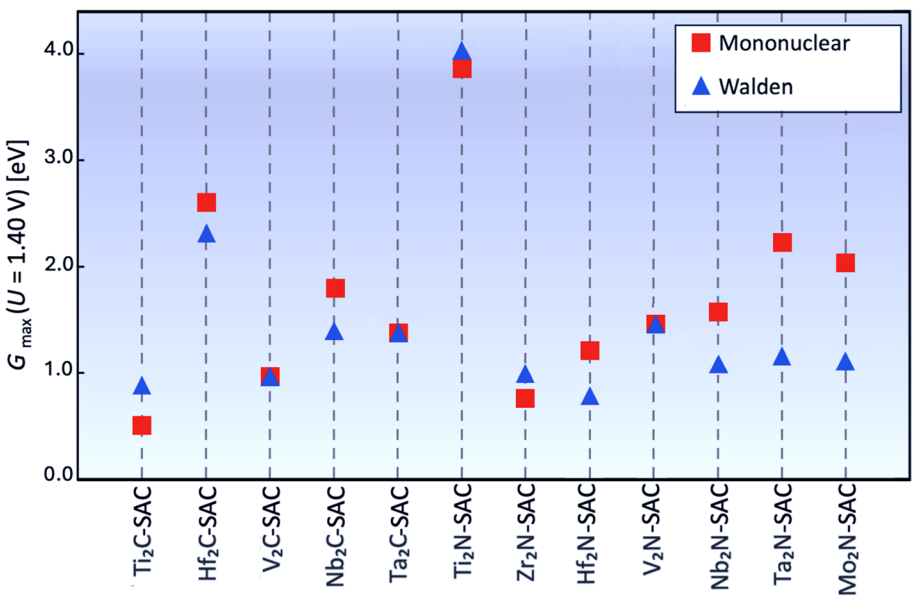

Fig. 4 Comparison of $G_{max}^{OER}(U)$ values for the mononuclear and Walden mechanisms (*cf.* Fig. 3) of twelve double-branch MXene-SAC motifs at $U = 1.40$ V *vs.* RHE to identify the preferred OER mechanism.

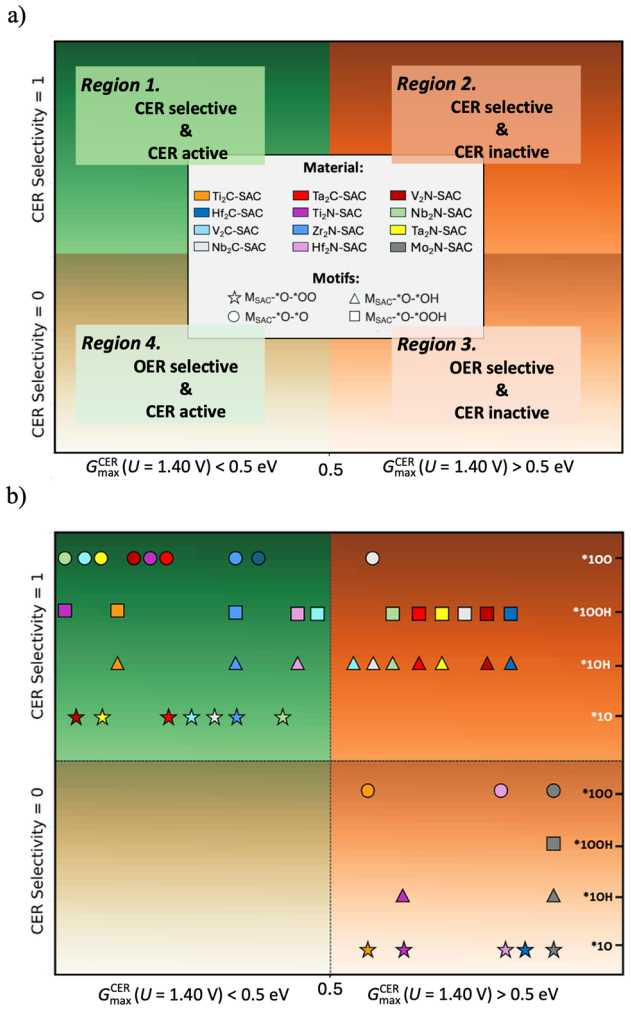

Fig. 5 Activity-selectivity map for the competing chlorine evolution (CER) and oxygen evolution (OER) reactions over two-branch MXene-SAC at $U = 1.40$ V *vs.* RHE. (a) Classification of four regions with different CER activity and selectivity. (b) Categorization of 48 different structures based on the double-branch MXene-SAC motif (*cf.* Fig. 1b) according to their CER activity and selectivity.

On the other hand, the presence of the *O and *OO adsorbates at the OER branch can also result in low CER activity and selectivity (motif in region 4) compared to the *OH and *OOH intermediates. Overall, the selectivity is only in favor of OER over CER in about 23% (11 of 48) of all surface states considered. While the above analysis refers to $U = 1.40$ V *vs.* RHE, we refer to section 5 of the SI for a potential-dependent analysis of the CER selectivity (*cf.* Fig. S18†). There, we demonstrate that the general trends discussed for $U = 1.40$ V *vs.* RHE (*cf.* Fig. 5) are not affected in the potential regime where the MXene-SAC is reported to be stable.[26]

Regarding the metal atom in the twelve different MXene-SAC motifs, we emphasize that there are seven MXenes — V_2C, Nb_2C, Ta_2C, V_2N, Zr_2N, Nb_2N, and Ta_2N — that maintain high CER selectivity throughout the catalytic cycle regardless of the adsorbate on the OER branch. On the other hand, for the other six MXenes — Ti_2C, Hf_2C, Ti_2N, Hf_2N, V_2N, and Mo_2N — we observe that some of the surface states are selective for the CER, while others favor the OER. This limits the application of the electrochemically formed SAC-like sites of the latter MXenes for selective CER, while especially group V-based MXenes (V_2X, Nb_2X, and Ta_2X) appear as promising candidates for experimental testing.

Finally, we comment on the structural properties of the double-branch MXene-SAC motif (*cf.* Fig. 1b) with regard to previous studies in the literature. As shown by previous work, it is important to consider the stacking and oxygen coverage of MXenes to properly describe thermal catalytic and electrocatalytic processes.[64] Single-atom catalysis on the oxygen-covered surface of MXenes has been largely realized by the doping with foreign metal atoms.[65,66] While single atoms on the surface of MXenes have shown to be a realistic description for thermal catalytic processes at the solid/gas interface,[67] a different situation is encountered in electrocatalysis, where the solid/liquid interface causes reconstruction of the oxygen-covered surface of MXenes under formation of the MXene-SAC motif (*cf.* Fig. 1). While the use of simplified SAC models based on doping with foreign metal atoms is still widely used in the theoretical description of electrocatalytic processes,[14,15] these models are likely not tenable under the harsh anodic conditions of CER and OER due to the reconstruction of the MXene surface. Therefore, the reported MXene-SAC motif not only refrains from rare noble metal atoms to enable efficient and selective catalysis similar to the actual functioning of SAC, but also is a better representation of MXenes in an electrochemical environment.

Conclusions

In summary, we have provided trends in the competing CER and OER at two-branch MXene-SAC sites by using electronic structure theory calculation in the DFT framework coupled with a descriptor-based analysis. Although previous works have outlined the application of MXenes in the form of composite catalysts with transition-metal oxides for selective CER or seawater splitting,[68–70] we demonstrate herein that *in situ* formed SAC sites of group V-based MXenes (V_2X, Nb_2X, and Ta_2X) are potential candidates for CER. While single-atom catalysts based on traditional synthesis routes are considered a game changer for selective chlorine evolution in slightly acidic media,[71–74] we propose the application of electrochemically formed SAC-like sites based on low-cost two-dimensional materials such as MXenes. This could help to overcome the dependence on rare precious metals, such as Pt and Ir in SAC catalysts or Ru and Ir in conventional heterogeneous catalysts, for energy conversion processes relevant to the chemical industry.

Data availability

The data supporting this article have been included as part of the ESI.†

Conflicts of interest

There are no conflicts to declare.

Acknowledgements

S. F., S. R., D. S., and K. S. E. thank the Ministry of Culture and Science of the Federal State of North Rhine-Westphalia (NRW Return Grant) for financial support to carry out this study. K. S. E. acknowledges funding by the RESOLV Cluster of Excellence, funded by the Deutsche Forschungsgemeinschaft under Germany's Excellence Strategy, EXC 2033-390677874, RE-SOLV. F. V. and F. I. acknowledge the Spanish Ministerio de Ciencia e Innovación and Agencia Estatal de Investigación (AEI) MCIN/AEI/10.13039/501100011033 and, as appropriate, by "European Union Next Generation EU/PRTR", through grant PID2021-126076NB-I00, la Unidad de Excelencia María de Maeztu CEX2021-001202-M granted to the ITQCUB and, in part, from COST Action CA18234 and Generalitat de Catalunya 2021SGR00079 grant. F. V. is thankful for the ICREA Academia Award 2023 ref. Ac2216561. L.M. thanks the China Scholarship Council (CSC) for financing her PhD (CSC202108390032).

References

1 S. Venkateshalu, M. Shariq, B. Kim, M. Patel, K. S. Mahabari, S.-I. Choi, N. K. Chaudhari, A. N. Grace and K. Lee, Recent Advances in MXenes: Beyond Ti-Only Systems, *J. Mater. Chem. A*, 2023, **11**(25), 13107–13132, DOI: **10.1039/D3TA01590D**.

2 M. Downes, C. E. Shuck, R. W. Lord, M. Anayee, M. Shekhirev, R. J. Wang, T. Hryhorchuk, M. Dahlqvist, J. Rosen and Y. Gogotsi, M_5X_4 : A Family of MXenes, *ACS Nano*, 2023, **17**(17), 17158–17168, DOI: **10.1021/acsnano.3c04967**.

3 M. Naguib, M. Kurtoglu, V. Presser, J. Lu, J. Niu, M. Heon, L. Hultman, Y. Gogotsi and M. W. Barsoum, Two-Dimensional Nanocrystals Produced by Exfoliation of Ti_3AlC_2, *Adv. Mater.*, 2011, **23**(37), 4248–4253, DOI: **10.1002/adma.201102306**.

4 B. Anasori, M. R. Lukatskaya and Y. Gogotsi, 2D Metal Carbides and Nitrides (MXenes) for Energy Storage, *Nat. Rev. Mater.*, 2017, **2**(2), 16098, DOI: **10.1038/natrevmats.2016.98**.

5 Y. Gogotsi and B. Anasori, The Rise of MXenes, *ACS Nano*, 2019, **13**(8), 8491–8494, DOI: **10.1021/acsnano.9b06394**.

6 T. Yang, J. Zhou, T. T. Song, L. Shen, Y. P. Feng and M. Yang, High-Throughput Identification of Exfoliable Two-Dimensional Materials with Active Basal Planes for Hydrogen Evolution, *ACS Energy Lett.*, 2020, **5**(7), 2313–2321, DOI: **10.1021/acsenergylett.0c00957**.

7 N. Karmodak and O. Andreussi, Catalytic Activity and Stability of Two-Dimensional Materials for the Hydrogen Evolution Reaction, *ACS Energy Lett.*, 2020, **5**(3), 885–891, DOI: **10.1021/acsenergylett.9b02689**.

8 Á. Morales-García, F. Calle-Vallejo and F. Illas, MXenes: New Horizons in Catalysis, *ACS Catal.*, 2020, **10**(22), 13487–13503, DOI: **10.1021/acscatal.0c03106**.

9 Y. Zhang, Y. Wang, N. Ma, B. Liang, Y. Xiong and J. Fan, Revealing the Adsorption Behavior of Nitrogen Reduction Reaction on Strained Ti_2CO_2 by a Spin-Polarized d-band Center Model, *Small*, 2024, **20**(9), 2306840, DOI: **10.1002/smll.202306840**.

10 D. Kan, D. Wang, X. Zhang, R. Lian, J. Xu, G. Chen and Y. Wei, Rational Design of Bifunctional ORR/OER Catalysts Based on Pt/Pd-Doped Nb_2CT_2 MXene by First-Principles Calculations, *J. Mater. Chem. A*, 2020, **8**(6), 3097–3108, DOI: **10.1039/C9TA12255A**.

11 X. Zhang, J. Lei, D. Wu, X. Zhao, Y. Jing and Z. Zhou, A Ti-Anchored Ti_2CO_2 Monolayer (MXene) as a Single-Atom Catalyst for CO Oxidation, *J. Mater. Chem. A*, 2016, **4**(13), 4871–4876, DOI: **10.1039/C6TA00554C**.

12 B. Huang, N. Li, W.-J. Ong and N. Zhou, Single Atom-Supported MXene: How Single-Atomic-Site Catalysts Tune the High Activity and Selectivity of Electrochemical Nitrogen Fixation, *J. Mater. Chem. A*, 2019, **7**(48), 27620–27631, DOI: **10.1039/C9TA09776G**.

13 A. D. Handoko, K. H. Khoo, T. L. Tan, H. Jin and Z. W. Seh, Establishing New Scaling Relations on Two-Dimensional MXenes for CO_2 Electroreduction, *J. Mater. Chem. A*, 2018, **6**(44), 21885–21890, DOI: **10.1039/C8TA06567E**.

14 D. Kan, R. Lian, D. Wang, X. Zhang, J. Xu, X. Gao, Y. Yu, G. Chen and Y. Wei, Screening Effective Single-Atom ORR and OER Electrocatalysts from Pt Decorated MXenes by First-Principles Calculations, *J. Mater. Chem. A*, 2020, **8**(33), 17065–17077, DOI: **10.1039/D0TA04429F**.

15 S. Venkateshalu, M. Shariq, B. Kim, M. Patel, K. S. Mahabari, S.-I. Choi, N. K. Chaudhari, A. N. Grace and K. Lee, Recent Advances in MXenes: Beyond Ti-Only Systems, *J. Mater. Chem. A*, 2023, **11**(25), 13107–13132, DOI: **10.1039/D3TA01590D**.

16 Z. W. Seh, K. D. Fredrickson, B. Anasori, J. Kibsgaard, A. L. Strickler, M. R. Lukatskaya, Y. Gogotsi, T. F. Jaramillo and A. Vojvodic, Two-Dimensional Molybdenum Carbide (MXene) as an Efficient Electrocatalyst for Hydrogen Evolution, *ACS Energy Lett.*, 2016, **1**(3), 589–594, DOI: **10.1021/acsenergylett.6b00247**.

17 M. Pandey and K. S. Thygesen, Two-Dimensional MXenes as Catalysts for Electrochemical Hydrogen Evolution: A Computational Screening Study, *J. Phys. Chem. C*, 2017, **121**(25), 13593–13598, DOI: **10.1021/acs.jpcc.7b05270**.

18 J. Zheng, X. Sun, C. Qiu, Y. Yan, Z. Yao, S. Deng, X. Zhong, G. Zhuang, Z. Wei and J. Wang, High-Throughput Screening of Hydrogen Evolution Reaction Catalysts in MXene Materials, *J. Phys. Chem. C*, 2020, **124**(25), 13695–13705, DOI: **10.1021/acs.jpcc.0c02265**.

19 D. Jin, L. R. Johnson, A. S. Raman, X. Ming, Y. Gao, F. Du, Y. Wei, G. Chen, A. Vojvodic, Y. Gogotsi and X. Meng, Computational Screening of 2D Ordered Double Transition-Metal Carbides (MXenes) as Electrocatalysts for Hydrogen Evolution Reaction, *J. Phys. Chem. C*, 2020, **124**(19), 10584–10592, DOI: **10.1021/acs.jpcc.0c01460**.

20 L. R. Johnson, S. Sridhar, L. Zhang, K. D. Fredrickson, A. S. Raman, J. Jang, C. Leach, A. Padmanabhan, C. C. Price, N. C. Frey, A. Raizada, V. Rajaraman, S. A. Saiprasad, X. Tang and A. Vojvodic, MXene Materials for the Electrochemical Nitrogen Reduction—

Functionalized or Not?, *ACS Catal.*, 2020, **10**(1), 253–264, DOI: 10.1021/acscatal.9b01925.

21 J. D. Gouveia, Á. Morales-García, F. Viñes, J. R. B. Gomes and F. Illas, Facile Heterogeneously Catalyzed Nitrogen Fixation by MXenes, *ACS Catal.*, 2020, **10**(9), 5049–5056, DOI: 10.1021/acscatal.0c00935.

22 T. Wu, P. R. C. Kent, Y. Gogotsi and D. Jiang, How Water Attacks MXene, *Chem. Mater.*, 2022, **34**(11), 4975–4982, DOI: 10.1021/acs.chemmater.2c00224.

23 P. Hou, Y. Tian, Y. Xie, F. Du, G. Chen, A. Vojvodic, J. Wu and X. Meng, Unraveling the Oxidation Behaviors of MXenes in Aqueous Systems by Active-Learning-Potential Molecular-Dynamics Simulation, *Angew. Chem., Int. Ed.*, 2023, **62**(32), e202304205, DOI: 10.1002/anie.202304205.

24 Y. Tian, P. Hou, H. Zhang, Y. Xie, G. Chen, Q. Li, F. Du, A. Vojvodic, J. Wu and X. Meng, Theoretical Insights on Potential-Dependent Oxidation Behaviors and Antioxidant Strategies of MXenes, *Nat. Commun.*, 2024, **15**(1), 10099, DOI: 10.1038/s41467-024-54455-z.

25 S. Razzaq, S. Faridi, S. Kenmoe, M. Usama, D. Singh, L. Meng, F. Vines, F. Illas and K. S. Exner, MXenes Spontaneously Form Active and Selective Single-Atom Centers under Anodic Polarization Conditions, *J. Am. Chem. Soc.*, 2025, **147**(1), 161–168, DOI: 10.1021/jacs.4c08518.

26 P. Wan, Y. Chen and Q. Tang, Electrochemical Stability of MXenes in Water Based on Constant Potential AIMD Simulations, *ChemPhysChem*, 2024, e202400325, DOI: 10.1002/cphc.202400325.

27 K. S. Exner, T. Lim and S. H. Joo, Circumventing the OCl *versus* OOH Scaling Relation in the Chlorine Evolution Reaction: Beyond Dimensionally Stable Anodes, *Curr. Opin. Electrochem.*, 2022, **34**, 100979, DOI: 10.1016/j.coelec.2022.100979.

28 Z. Deng, S. Xu, C. Liu, X. Zhang, M. Li and Z. Zhao, Stability of Dimensionally Stable Anode for Chlorine Evolution Reaction, *Nano Res.*, 2024, **17**(3), 949–959, DOI: 10.1007/s12274-023-5965-7.

29 R. K. B. Karlsson and A. Cornell, Selectivity between Oxygen and Chlorine Evolution in the Chlor-Alkali and Chlorate Processes, *Chem. Rev.*, 2016, **116**(5), 2982–3028, DOI: 10.1021/acs.chemrev.5b00389.

30 C. Saetta, I. Barlocco, G. D. Liberto and G. Pacchioni, Key Ingredients for the Screening of Single Atom Catalysts for the Hydrogen Evolution Reaction: The Case of Titanium Nitride, *Small*, 2024, **20**(37), 2401058, DOI: 10.1002/smll.202401058.

31 N. Allasia, S. Xu, S. F. Jafri, E. Borfecchia, L. A. Cipriano, G. Terraneo, S. Tosoni, L. Mino, G. Di Liberto, G. Pacchioni and G. Vilé, Resolving the Nanostructure of Carbon Nitride-Supported Single-Atom Catalysts, *Small*, 2025, 2408286, DOI: 10.1002/smll.202408286.

32 X.-F. Yang, A. Wang, B. Qiao, J. Li, J. Liu and T. Zhang, Single-Atom Catalysts: A New Frontier in Heterogeneous Catalysis, *Acc. Chem. Res.*, 2013, **46**(8), 1740–1748, DOI: 10.1021/ar300361m.

33 J. Kim, M. Usama, K. S. Exner and S. H. Joo, Renaissance of Chlorine Evolution Reaction: Emerging Theory and Catalytic Materials, *Angew. Chem., Int. Ed.*, 2025, **64**(1), e202417293, DOI: 10.1002/anie.202417293.

34 J. G. Vos, T. A. Wezendonk, A. W. Jeremiasse and M. T. M. Koper, MnO_x/IrO_x as Selective Oxygen Evolution Electrocatalyst in Acidic Chloride Solution, *J. Am. Chem. Soc.*, 2018, **140**(32), 10270–10281, DOI: 10.1021/jacs.8b05382.

35 J. G. Vos and M. T. M. Koper, Measurement of Competition between Oxygen Evolution and Chlorine Evolution Using Rotating Ring-Disk Electrode Voltammetry, *J. Electroanal. Chem.*, 2018, **819**, 260–268, DOI: 10.1016/j.jelechem.2017.10.058.

36 S. Trasatti, Electrocatalysis: Understanding the Success of DSA®, *Electrochim. Acta*, 2000, **45**(15), 2377–2385, DOI: 10.1016/S0013-4686(00)00338-8.

37 T. Lim, G. Y. Jung, J. H. Kim, S. O. Park, J. Park, Y.-T. Kim, S. J. Kang, H. Y. Jeong, S. K. Kwak and S. H. Joo, Atomically Dispersed Pt–N4 Sites as Efficient and Selective Electrocatalysts for the Chlorine Evolution Reaction, *Nat. Commun.*, 2020, **11**(1), 412, DOI: 10.1038/s41467-019-14272-1.

38 J. D. Gouveia, F. Viñes, F. Illas and J. R. B. Gomes, MXenes Atomic Layer Stacking Phase Transitions and Their Chemical Activity Consequences, *Phys. Rev. Mater.*, 2020, **4**(5), 054003, DOI: 10.1103/PhysRevMaterials.4.054003.

39 G. Kresse and J. Furthmüller, Efficient Iterative Schemes for *Ab Initio* Total-Energy Calculations Using a Plane-Wave Basis Set, *Phys. Rev. B*, 1996, **54**(16), 11169–11186, DOI: 10.1103/PhysRevB.54.11169.

40 G. Kresse and J. Furthmüller, Efficiency of *Ab Initio* Total Energy Calculations for Metals and Semiconductors Using a Plane-Wave Basis Set, *Comput. Mater. Sci.*, 1996, **6**(1), 15–50, DOI: 10.1016/0927-0256(96)00008-0.

41 G. Kresse and J. Hafner, *Ab Initio* Molecular Dynamics for Liquid Metals, *Phys. Rev. B*, 1993, **47**(1), 558–561, DOI: 10.1103/PhysRevB.47.558.

42 J. P. Perdew, K. Burke and M. Ernzerhof, Generalized Gradient Approximation Made Simple, *Phys. Rev. Lett.*, 1996, **77**(18), 3865–3868, DOI: 10.1103/PhysRevLett.77.3865.

43 S. Grimme, J. Antony, S. Ehrlich and H. Krieg, A Consistent and Accurate *Ab Initio* Parametrization of Density Functional Dispersion Correction (DFT-D) for the 94 Elements H-Pu, *J. Chem. Phys.*, 2010, **132**(15), 154104, DOI: 10.1063/1.3382344.

44 G. Kresse and D. Joubert, From Ultrasoft Pseudopotentials to the Projector Augmented-Wave Method, *Phys. Rev. B*, 1999, **59**(3), 1758–1775, DOI: 10.1103/PhysRevB.59.1758.

45 M. López, K. S. Exner, F. Viñes and F. Illas, Computational Pourbaix Diagrams for MXenes: A Key Ingredient toward Proper Theoretical Electrocatalytic Studies, *Adv. Theory Simul.*, 2023, **6**(10), 2200217, DOI: 10.1002/adts.202200217.

46 S. Razzaq, S. Faridi, S. Kenmoe, M. Usama, D. Singh, L. Meng, F. Vines, F. Illas and K. S. Exner, MXenes Spontaneously Form Active and Selective Single-Atom Centers under Anodic Polarization Conditions, *J. Am. Chem. Soc.*, 2025, **147**, 161–168, DOI: 10.1021/jacs.4c08518.

47 J. K. Nørskov, J. Rossmeisl, A. Logadottir, L. Lindqvist, J. R. Kitchin, T. Bligaard and H. Jónsson, Origin of the Overpotential for Oxygen Reduction at a Fuel-Cell Cathode, *J. Phys. Chem. B*, 2004, **108**(46), 17886–17892, DOI: 10.1021/jp047349j.

48 D. Ontiveros, S. Vela, F. Viñes and C. Sousa, Tuning MXenes Towards Their Use in Photocatalytic Water Splitting, *Energy Environ. Mater.*, 2024, **7**(6), e12774, DOI: 10.1002/eem2.12774.

49 L. A. Cipriano, G. Di Liberto and G. Pacchioni, Superoxo and Peroxo Complexes on Single-Atom Catalysts: Impact on the Oxygen Evolution Reaction, *ACS Catal.*, 2022, **12**(19), 11682–11691, DOI: 10.1021/acscatal.2c03020.

50 G. Di Liberto and G. Pacchioni, Modeling Single-Atom Catalysis, *Adv. Mater.*, 2023, **35**(46), 2307150, DOI: 10.1002/adma.202307150.

51 L. Zhong and S. Li, Unconventional Oxygen Reduction Reaction Mechanism and Scaling Relation on Single-Atom Catalysts, *ACS Catal.*, 2020, **10**(7), 4313–4318, DOI: 10.1021/acscatal.0c00815.

52 H. A. Hansen, J. Rossmeisl and J. K. Nørskov, Surface Pourbaix Diagrams and Oxygen Reduction Activity of Pt, Ag and Ni(111) Surfaces Studied by DFT, *Phys. Chem. Chem. Phys.*, 2008, **10**(25), 3722, DOI: 10.1039/b803956a.

53 O. Vinogradova, D. Krishnamurthy, V. Pande and V. Viswanathan, Quantifying Confidence in DFT-Predicted Surface Pourbaix Diagrams of Transition-Metal Electrode–Electrolyte Interfaces, *Langmuir*, 2018, **34**(41), 12259–12269, DOI: 10.1021/acs.langmuir.8b02219.

54 V. Sumaria, D. Krishnamurthy and V. Viswanathan, Quantifying Confidence in DFT Predicted Surface Pourbaix Diagrams and Associated Reaction Pathways for Chlorine Evolution, *ACS Catal.*, 2018, **8**(10), 9034–9042, DOI: 10.1021/acscatal.8b01432.

55 I. Barlocco, L. A. Cipriano, G. Di Liberto and G. Pacchioni, Does the Oxygen Evolution Reaction Follow the Classical OH*, O*, OOH* Path on Single Atom Catalysts?, *J. Catal.*, 2023, **417**, 351–359, DOI: 10.1016/j.jcat.2022.12.014.

56 S. Yu, Z. Levell, Z. Jiang, X. Zhao and Y. Liu, What Is the Rate-Limiting Step of Oxygen Reduction Reaction on Fe–N–C Catalysts?, *J. Am. Chem. Soc.*, 2023, **145**(46), 25352–25356, DOI: 10.1021/jacs.3c09193.

57 K. S. Exner, Importance of the Walden Inversion for the Activity Volcano Plot of Oxygen Evolution, *Adv. Sci.*, 2023, **10**(36), 2305505, DOI: 10.1002/advs.202305505.

58 K. S. Exner, Four Generations of Volcano Plots for the Oxygen Evolution Reaction: Beyond Proton-Coupled Electron Transfer Steps?, *Acc. Chem. Res.*, 2024, **57**(9), 1336–1345, DOI: 10.1021/acs.accounts.4c00048.

59 H. A. Hansen, I. C. Man, F. Studt, F. Abild-Pedersen, T. Bligaard and J. Rossmeisl, Electrochemical Chlorine Evolution at Rutile Oxide (110) Surfaces, *Phys. Chem. Chem. Phys.*, 2010, **12**(1), 283–290, DOI: 10.1039/B917459A.

60 K. S. Exner, A Universal Descriptor for the Screening of Electrode Materials for Multiple-Electron Processes: Beyond the Thermodynamic Overpotential, *ACS Catal.*, 2020, **10**(21), 12607–12617, DOI: 10.1021/acscatal.0c03865.

61 S. Razzaq and K. S. Exner, Materials Screening by the Descriptor G_{max} (η): The Free-Energy Span Model in Electrocatalysis, *ACS Catal.*, 2023, **13**(3), 1740–1758, DOI: 10.1021/acscatal.2c03997.

62 S. Kozuch and S. Shaik, How to Conceptualize Catalytic Cycles? The Energetic Span Model, *Acc. Chem. Res.*, 2011, **44**(2), 101–110, DOI: 10.1021/ar1000956.

63 K. S. Exner, Controlling Stability and Selectivity in the Competing Chlorine and Oxygen Evolution Reaction over Transition Metal Oxide Electrodes, *ChemElectroChem*, 2019, **6**(13), 3401–3409, DOI: 10.1002/celc.201900834.

64 Á. Morales-García, J. D. Gouveia, A. V. López, A. Comas-Vives, F. Viñes, J. R. B. Gomes and F. Illas, MXene Termination and Stacking Bias on the Reverse Water Gas Shift Reaction Catalysis, *Mater. Today Catal.*, 2024, **7**, 100076, DOI: 10.1016/j.mtcata.2024.100076.

65 H. Q. Pham and T. T. Huynh, Applications of Doped-MXene-Based Materials for Electrochemical Energy Storage, *Coord. Chem. Rev.*, 2024, **517**, 216039, DOI: 10.1016/j.ccr.2024.216039.

66 J. Zhou, M. Dahlqvist, J. Björk and J. Rosen, Atomic Scale Design of MXenes and Their Parent Materials—From Theoretical and Experimental Perspectives, *Chem. Rev.*, 2023, **123**(23), 13291–13322, DOI: 10.1021/acs.chemrev.3c00241.

67 H. Zhou, Z. Chen, A. V. López, E. D. López, E. Lam, A. Tsoukalou, E. Willinger, D. A. Kuznetsov, D. Mance, A. Kierzkowska, F. Donat, P. M. Abdala, A. Comas-Vives, C. Copéret, A. Fedorov and C. R. Müller, Engineering the Cu/Mo2CT$_x$ (MXene) Interface to Drive CO2 Hydrogenation to Methanol, *Nat. Catal.*, 2021, **4**(10), 860–871, DOI: 10.1038/s41929-021-00684-0.

68 S. Gbadamasi, S. Loomba, M. Haris, M. W. Khan, A. Maibam, S. M. Mousavi, S. Mahmud, L. Thomsen, A. Tadich, R. Babarao, J. Xian and N. Mahmood, Breaking the Inactivity of MXenes to Drive Ampere-Level Selective Oxygen Evolution Reaction in Seawater, *Mater. Sci. Eng. R Rep.*, 2024, **160**, 100835, DOI: 10.1016/j.mser.2024.100835.

69 Y. Duan, L. Wei, C. Cai, J. Mi, F. Cao, J. Chen, X. Li, X. Pang, B. Li and L. Wang, RuO2/TiO2/MXene with Multi-Heterojunctions Coating on Carbon Cloth for High-Activity Chlorine Evolution Reaction at Large Current Densities, *Nano Res.*, 2024, **17**(6), 4764–4772, DOI: 10.1007/s12274-024-6419-6.

70 B. Li, Y. Duan, L. Wei, C. Cai, J. Zhu, J. Mi, H. Li, X. Pang and L. Wang, 2D MXene Ti_3C_2 Coupled with 1D Co_3O_4 Nanowires on Carbon Cloth for Efficient Chlorine Evolution Activity, *Adv. Funct. Mater.*, 2024, **34**(24), 2314150, DOI: 10.1002/adfm.202314150.

71 L. Quan, X. Chen, J. Liu, S. Fan, B. Y. Xia and B. You, Atomic Pt-N_4 Sites in Porous N-Doped Nanocarbons for Enhanced On-Site Chlorination Coupled with H_2 Evolution in Acidic Water, *Adv. Funct. Mater.*, 2023, **33**(41), 2307643, DOI: 10.1002/adfm.202307643.

72 J. H. Kim and S. H. Joo, Rise of Atomically Dispersed Metal Catalysts: Are They a New Class of Catalysts?, *Bull. Korean Chem. Soc.*, 2024, **45**(4), 350–358, DOI: 10.1002/bkcs.12830.

73 L. Quan, X. Zhao, L. Yang, B. You and B. Y. Xia, Intrinsic Activity Identification of Noble Metal Single-Sites for Electrocatalytic Chlorine Evolution, *Angew. Chem., Int. Ed.*, 2024, e202414202, DOI: **10.1002/anie.202414202**.

74 J. H. Kim, Y. J. Sa, T. Lim, J. Woo and S. H. Joo, Steering Catalytic Selectivity with Atomically Dispersed Metal Electrocatalysts for Renewable Energy Conversion and Commodity Chemical Production, *Acc. Chem. Res.*, 2022, **55**(18), 2672–2684, DOI: **10.1021/acs.accounts.2c00409**.